Chemical Papers (2020) 74:619–630
https://doi.org/10.1007/s11696-019-00906-7

ORIGINAL PAPER

Sorption and possible preconcentration of europium and gadolinium ions from aqueous solutions by Mn_3O_4 nanoparticles

Moubarak A. Sayed[1,3] · A. I. Helal[1] · S. M. Abdelwahab[2] · H. H. Mahmoud[1,4] · H. F. Aly[3]

Received: 8 April 2019 / Accepted: 13 August 2019 / Published online: 22 August 2019

Abstract

Mn_3O_4 nanoparticles were prepared by co-precipitation method. The prepared samples had been characterized to find the compositional, structural, and functional properties, by means of EDX, XRD, and FTIR, respectively. The prepared manganese oxide nanoparticles (Mn_3O_4 NPs) have average crystallite size of 30–35 nm. The effect of different parameters on the uptake of Eu(III) and Gd(III) by Mn_3O_4 nanoparticles such as pH, initial metal concentration, shaking time, and temperature was examined. The shaking time for both adsorption and desorption was found to be 5 h. The sorption capacities at equilibrium with regards to Eu(III) and Gd(III) were 26.8 and 12.6 mg/g, respectively. Kinetically, the sorption of both elements fitted well to pseudo-second-order model. Sorption equilibrium isotherm obeys more favorably the Langmuir isotherm model. Desorption process of Eu(III) and Gd(III) from Mn_3O_4 NPs was highly managed using 2.0 M HNO_3. A preconcentration factor of 70 and 20 was obtained for Gd and Eu, respectively, using 0.1 g of the Mn_3O_4 nanoparticles.

Keywords Mn_3O_4 nanoparticles · Co-precipitation · Crystallite size · Gadolinium · Europium · Preconcentration

Introduction

Gadolinium is usually considered as one of the lanthanide series in the periodic table, and it has a lot of uses in the field of structural components, fluorescent materials, mechanical devices, electronic industry, and nuclear industry (Singha et al. 2014). Gadolinium is frequently found in nature in two alternative types of ores such as bastnasite and monazite (Zamani et al. 2012). In nuclear field, gadolinium is used as a neutron absorber concerning the control level regulations of nuclear reactors (Rufus et al. 2018). Gd-153 isotope is utilized in X-ray fluorescence in addition to osteoporosis screening. Gadolinium is a gamma-emitter including half-life time about 8 months, so it is applicable for medical disciplines (Othersen et al. 2007). As consequence of utilizing radiotracers, they may leak into the encompassing environment causing poisonous impacts such as radioactive contamination. In addition, radiotracers may lead to a great damage to the body organs as a result of direct contact during treatment or in other methods applied to human beings (Singha et al. 2014).

Europium radioisotopes are used as burn-up monitors to assess the performance of reactors fuels (Kazakov et al. 2018). Europium is used in several fields such as material science and electronics. The struggle between growing requirement in a variety of industries and also the restricted amount of Gd(III) and Eu(III) resulted in an excessive growth in the demand for the recovery of both elements. Therefore, the determination, separation, and recovery of Eu(III) and Gd(III) are very critical due to their existence at very trace concentrations (Aghamohammadhasan et al. 2017).

There are many analytical instruments presented for the determination of gadolinium and europium in different industrial, geological, and environmental samples such as

Electronic supplementary material The online version of this article (https://doi.org/10.1007/s11696-019-00906-7) contains supplementary material, which is available to authorized users.

✉ Moubarak A. Sayed
mom467@usask.ca

[1] Central Laboratory for Elemental and Isotopic Analysis, Nuclear Research Centre, Atomic Energy Authority, Inshas, Cairo, Egypt

[2] Chemistry Department, Faculty of Science, Ain-shams University, Cairo, Egypt

[3] Hot Laboratories Center, Atomic Energy Authority, Inshas, Cairo 13759, Egypt

[4] Radioisotope Department, Nuclear Research Center, Atomic Energy Authority, Dokki, Giza 12311, Egypt

inductively coupled plasma optical emission spectrometry (ICP-OES) (Li and Hu 2010), electron spin resonance (ESR) (Moyer and McCarthy 1969), spectrofluorometry (Aghamohammadhasan et al. 2017), and neutron activation analysis (Bartolini et al. 2003). Despite the exceptional development of instrumental strength for detection and determination of trace elements, the determination of gadolinium and europium in trace concentrations by recent analytical techniques is, in many cases, difficult (Shizhong et al. 2007). This is not solely as a result of the deficient sensitivity of the methods, but additionally due to the matrix interference (Kanna et al. 2005). So as to conquer these troubles, a lot of separation or preconcentration methods, for example, ion exchange, co-precipitation, solvent extraction, solid-phase extraction, resin chelation, etc., are still required preceding the analysis (Liang and Chen 2005).

Solid-phase extraction has grown to be the most widely recognized method for the determination of trace concentrations of REEs in diverse matrices as a result of its extraordinary recovery, little extraction time, and high enrichment factor as compared to liquid–liquid extraction (Liang et al. 2005). Many adsorbent materials, such as chelating resin (Person et al. 2011), modified Amberlite XAD-4 (Karadas et al. 2011), graphene oxide-TiO_2 composite (Zhang et al. 2015), and modified polystyrene (Fedyunina et al. 2012) have been proposed for separation and preconcentration of REEs. Among these adsorbents, nanomaterials are applied as adsorbents, with crystallite size less than 100 nm, because of their distinct mechanical, electronic, thermal, and biological properties (Pyrzynska 2013). Among these nanomaterials, trimanganese tetraoxide, Mn_3O_4 (hausmannite), is considered to be the maximum stable manganese oxide at high temperatures in contrast of other manganese oxides, for example, MnO_2 and Mn_2O_3 (Mansournia et al. 2015). Hausmannite is a brown to black metallic mineral (Bastami and Entezari 2010). At room temperature, it has spinel structure and a tetragonal phase, wherever the Mn^{3+} and Mn^{2+} ions occupy octahedral and tetrahedral positions within the spinel structure, respectively (Vázquez-Olmos et al. 2005; Belkhedkar and Ubale 2014). Furthermore, Mn_3O_4 has been applied for manufacturing of some magnetic materials like manganese zinc ferrite (Chen et al. 2014). Lately, a lot of interest has been devoted for the synthesis of manganese oxides nanoparticles. Mn_3O_4 NPs are widely applied in different applications such as catalysis (Lei et al. 2007), Ion exchange, molecular adsorption (Zhang et al. 2010) due to their structural flexibility and unique properties. Manganese oxide (Mn_3O_4 NP_s) is an important scavenger for heavy metal removal from soil, sediments, and rock because of its principal sorptive properties such as high porosity, large surface area, as well as the presence of more active sites for binding with metal ions (Liu et al. 2015).

In the previous studies, numerous materials have been used as solid-phase extractants for the preconcentration, recovery, and sorption of gadolinium such as modified silica (El-Sofany 2008), Amberlite (Gad et al. 2017), and gibbsite (Huittinen et al. 2009). Several adsorbents have been applied for the sorption and separation of Eu(III) such as imprinted polymer (Alizadeh and Amjadi 2013), 1-(2-pyridylazo)-2-naphthol (Mallah et al. 2008), di(2-ethylhexyl)phosphoric acid and Triton X-100 (Ohashi et al. 2007), and graphene oxide nanosheet (Sun et al. 2012). Till now, no research has so far been published regarding the use of Mn_3O_4 nanoparticles (Mn_3O_4 NPs) as sorbent for europium and gadolinium ions.

This work is focusing on the possible use of nano Mn_3O_4 as solid-phase extractant for the sorption and preconcentration of europium and gadolinium ions from aqueous solutions. The parameters affecting the sorption of gadolinium and europium like pH, shaking time, metal concentration, and temperature were examined. The obtained results are discussed according to different kinetic and isotherm models. Furthermore, the possible use of Mn_3O_4 for preconcentration of Gd and Eu from aqueous solutions was carried out and discussed.

Experimental

Synthesis of nanosized Mn_3O_4

The synthesis of Mn_3O_4 nanoparticles was performed using the co-precipitation method (Shrividhya et al. 2014). First, 1.0 M of $MnSO_4$. H_2O was dissolved in certain volume of de-ionized water, and then, 2.0 M of NaOH was added drop wise to the previous solution. Ammonia was added to adjust pH at 11 ± 0.2. To precipitate Mn_3O_4 nanoparticles, the solution should be stirred for 2 h at certain temperature (60 °C). The precipitated nanoparticles were gathered, washed with de-ionized water and ethanol 2–3 times, and dried in hot air oven at 100 °C for 12 h. Finally, Mn_3O_4 NPs were annealed for 2 h at 300 °C.

The formation of Mn_3O_4 nanoparticles in the alkaline aqueous solution may be described by Eqs. (1–3) (Dhaouadi et al. 2012):

$$Mn^{2+} + 2OH^- \rightarrow Mn(OH)_2, \quad (1)$$

$$Mn(OH)_2 \xrightarrow{100\ ^\circ C} MnO + H_2O, \quad (2)$$

$$3\ MnO + 0.5\ O_2 \xrightarrow{300\ ^\circ C} Mn_3O_4. \quad (3)$$

First, manganese ions are reduced in alkaline medium to $Mn(OH)_2$, secondly $Mn(OH)_2$ decomposed into MnO at 100 °C for 12 h, and finally, in the presence of atmospheric

oxygen at muffle furnace, MnO is oxidized to Mn_3O_4 at 300 °C.

Reagents

Manganese sulfate monohydrate (Sigma-Aldrich, USA) and sodium hydroxide (Sigma-Aldrich, USA) were used without purification. Standard stock solution of Gd (1000 mg/L) was used. Eu standard solution (1000 mg/L) was prepared by dissolving certain weight of Eu_2O_3 (Sigma-Aldrich, USA) in concentrated HNO_3 and diluting to the required volume with 18 MΩ de-ionized water.

Instrumentation

The characterization of nanosized Mn_3O_4 was conducted with several experimental techniques: X-ray diffraction (XRD) patterns of nanosized Mn_3O_4 were analyzed using BRUKER X-Ray Diffractometer (Germany) of type AXS D8 ADVANCE (Cu target, $\lambda = 1.540$ Å) in the range of $2\theta = 10°–80°$ at 40 kV potential and 40 Ma current. Elemental composition was detected by an Oxford energy-dispersive X-ray (EDX) spectrometer (Oxford Link ISIS) attached to the SEM (Model Jeol JSM-5600 LV) using a Si/Li detector with Be window. Transmission electron microscope (TEM) images of samples were obtained using a Hitachi HT-7700 microscope at voltage 100 kV. Samples were prepared by depositing a drop of colloidal suspension of sorbent in ethanol onto a carbon-coated copper TEM grid. The morphology of Mn_3O_4 NPs was examined using a Hitachi, SU8000-Field Emission Scanning Electron Microscope (FE-SEM). Fourier Transform Infrared (FTIR) spectra were obtained by a spectrometer (NICOLET iS10 model) within the wave number from 400 to 4000 cm^{-1} on KBr pellets. The initial concentration and final concentration of Gd(III) and Eu(III) were measured by Inductively Coupled Plasma Optical Emission Spectroscopy (ICP-OES), Prodigy, USA. Quantachrome, Nova 1100e series, version 2.1, USA, was utilized for determination of the surface area and porosity of Mn_3O_4 NPs. pH meter (Cyperscan 500 pH, USA) which was preliminary calibrated using suitable buffer solutions was used for measuring the pH value of aqueous solutions.

Procedures for sorption of Gd and Eu

The standard solutions of Gd or Eu ions (20–400 mg/l) were pipetted into different bottles. The solutions were adjusted in different pH values (3.0–10.0) using 0.01–0.1 M HCl and/or NaOH solutions. After that, the new sorbents Mn_3O_4 NPs were added with dose (0.01–0.25 g/20 ml) to Gd or Eu solution at room temperature of 25 °C. The mixture was vigorously shacked for prefixed time (5–300 min). After centrifugation, the residual gadolinium or europium ion concentration in the filtrate was analyzed by ICP-OES. The removal or uptake percentage (R %) can be calculated from the following equation:

$$R\% = \left(\frac{C_o - C_e}{C_o}\right) \times 100. \tag{4}$$

The sorption capacity of Gd(III) or Eu(III) ions by Mn_3O_4 NPs was calculated from the following equation:

$$q_e = \left(C_o - C_e\right) \times \frac{V}{m}, \tag{5}$$

where q_e (mg/g) is the amount of Gd(III) or Eu(III) adsorbed per unit mass of Mn_3O_4 NPs, C_o is the initial Gd(III) or Eu(III) concentration (mg/l), C_e is the equilibrium concentrations of Gd(III) or Eu(III) (mg/l), V (liters) is volume of Gd(III) or Eu(III) solution, and m (g) is the weight of sorbent.

Desorption procedures

Mn_3O_4 NPs were tested for their re-usability after the removal europium and gadolinium ions from aqueous solutions. After the adsorption experiment was carried out as previously mentioned in "Procedures for sorption of Gd and Eu", the metal-loaded Mn_3O_4 NPs were rinsed twice in de-ionized water, and then, different concentrations of hydrochloric acid, nitric acid, and EDTA were added as desorbent agents. The sample was shacked for specific time. Finally, the sample was centrifuged for 20 min at 6000 rpm and the filtrate was analyzed for the released concentration of Eu(III) or Gd(III) using ICP-OES.

The desorption efficiency was calculated using the following equation:

$$\text{Desorption efficiency (\%)} = \frac{\text{release metal concentration}}{\text{initially sorbed metal concetration}} \times 100. \tag{6}$$

Results and discussion

Characterization of Mn_3O_4 nanoparticles

The nanosized Mn_3O_4 used as sorbents was characterized in terms of chemical analysis and structural composition.

Chemical analysis

Energy-dispersive X-ray spectroscopy (EDX) The composition of synthesized Mn_3O_4 NPs was analyzed using energy-dispersive X-ray (EDX) spectrometer as shown in Fig. 1. From the results given in Fig. 1, it was concluded that the synthesized Mn_3O_4 was composed only from Mn and O. No

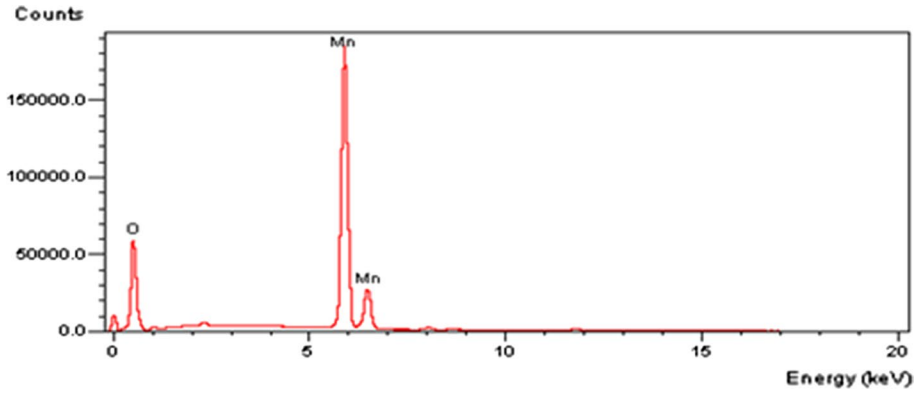

Fig. 1 EDX spectrum of Mn_3O_4 NPs

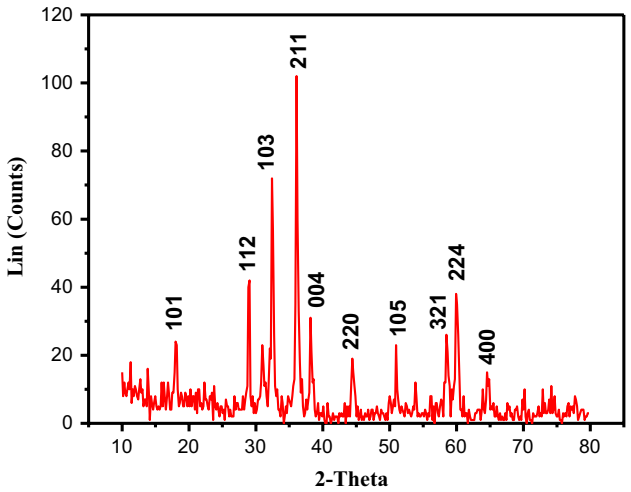

Fig. 2 XRD pattern of Mn_3O_4 NPs

other peaks for any elements as impurities have been found in the EDX spectrum, which demonstrates that the Mn_3O_4 NPs are of high purity.

Structural analysis

X-ray diffraction All the peaks of XRD pattern of Mn_3O_4 NPs (shown in Fig. 2) can be perfectly matched with the standard diffraction data of hausmannite structure of Mn_3O_4 [JCPDS Card 01-1127 (D)] and also matched well with literature data (Liu et al. 2015). In addition, no any peaks corresponding to impurity phases have been detected, indicating the high purity and good crystallinity of Mn_3O_4 NPs. Furthermore, the average crystallite size was measured to be 30–35 nm (as compared to 50 nm which was obtained by Dhaouadi et al. 2012) in relation to the five main peaks (112), (103), (211), (224), and (321) using the Debye–Scherrer equation, which is described as follows:

$$E = 0.9\,\lambda/\beta\,\cos\theta.$$

where E is the size of crystallite in nanometers, β (FWHM, radian) is the full width at half maximum, θ is the Bragg angle (°), and λ is the wave length of X-ray ($\lambda = 1.5418$ Å) (Dhaouadi et al. 2012).

Fourier transform infrared (FTIR) analysis The prepared Mn_3O_4 NPs were characterized by FTIR analysis, as shown in Fig. 3. Three bands were detected at 415,622 and 514 cm^{-1}, associated with the coupling between Mn–O stretching modes of tetrahedral and octahedral sites (Dubal et al. 2011), and this approves the formation of Mn_3O_4 NPs. In addition, the bands from 3500 to 1500 cm^{-1} m can be correlated to the vibration of O–H in the weakly bonded physisorbed water molecules. A wide band at around 3419 cm^{-1} was related to the stretching vibrations of the O–H bond. It was found that the other two weak peaks at 2344 cm^{-1} and 1638 cm^{-1} were totally assigned to the bending vibrations of O–H bond combined with Mn atoms. The peaks at 1117 cm^{-1} were due to the O–H-bending modes of γ–OH (Sherin et al. 2014). Consequently, the FTIR spectrum confirms the formation of Mn_3O_4 NPs and this outcome is in a good agreement with data obtained from X-ray diffraction. The IR spectra after the adsorption processes of Gd(III) and Eu(III) ions onto Mn_3O_4 NPs are also shown in Fig. 3. The FTIR spectrum explained that the peaks were slightly shifted towards higher value. This shift in peak values may be owing to the formation of chemical bond between functional groups present on Mn_3O_4 NPs and Eu(III) and Gd(III) (Sartape et al. 2017). The band shifting from 1638 up to 1654 cm^{-1}, from 1638 to 1634 cm^{-1}, and from 1117 to 1122 cm^{-1} and 1124 cm^{-1} may be due to the interaction between the O–H group of Mn_3O_4 NPs and Eu(III) and Gd(III). The appearance of the new sharp band around 1383 cm^{-1} can be apportioned to the O–H···O in-plane bending. The peaks around 410 cm^{-1}, 530 cm^{-1} and 630 cm^{-1} correspond to Mn–O–Eu as well as Mn–O–Gd bond, respectively (Al Lafi and Al Abdullah 2015).

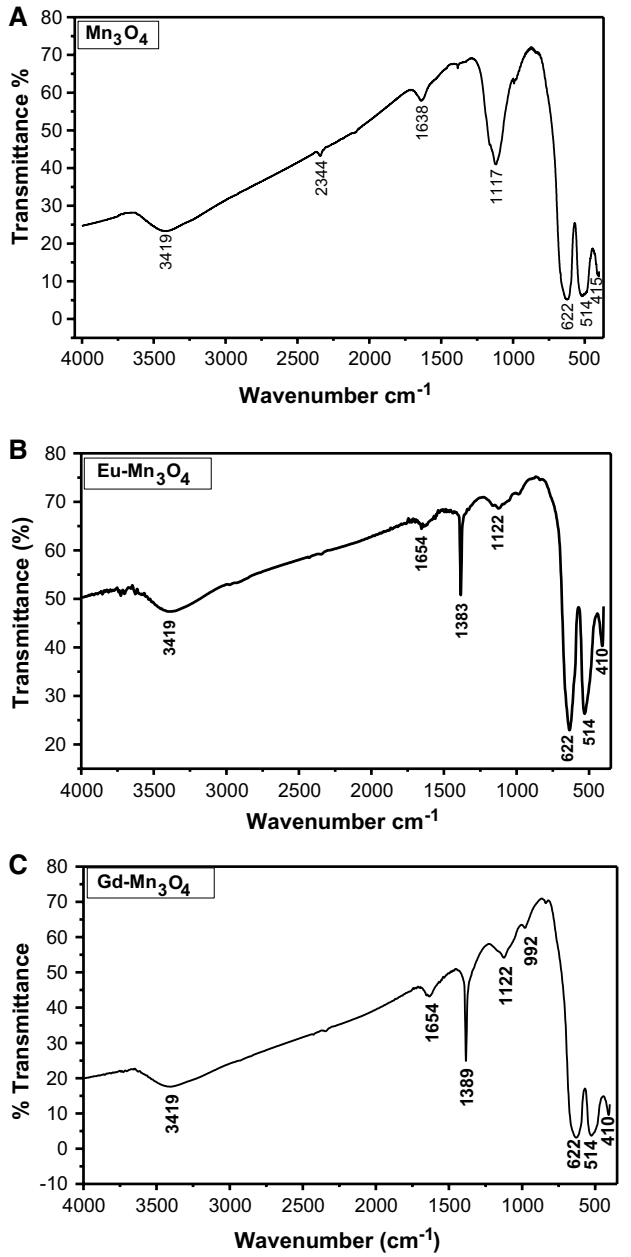

Fig. 3 FTIR spectrum of **a** Mn_3O_4 NPs before adsorption, **b** after adsorption of Eu(III), and **c** after adsorption of Gd(III)

Morphological study

FE-SEM and HR-TEM analysis The surface morphology of Mn_3O_4 NPs was studied using FE-SEM and HR-TEM. From SEM image given in Fig. 4a, it can be observed that the aggregated Mn_3O_4 NPs have nearly cubic like structure. From HR-TEM image in Fig. 4b, it was shown that the average diameter of Mn_3O_4 NPs was ranged from 30 to 32 nm. This value is in a good agreement with the data that was obtained from XRD.

Physical properties of Mn_3O_4 nanoparticles

The N_2 adsorption and desorption isotherm of synthesized Mn_3O_4 nanoparticles is given in Table S1 (See supplementary materials). The BET surface area of Mn_3O_4 was calculated to be 13.4 m^2/g. The pore diameter was detected in the range of 9.12 nm.

Point of zero charges (pHpzc) of Mn_3O_4 nanoparticles

pHpzc is the value of pH at which the net surface charge of Mn_3O_4 nanoparticles in aqueous solutions is zero. The procedures of pHpzc were determined according to the previously reported method by Dalvand et al. (2016). First, six bottles of volume of 20 mL of NaCl (0.01 M) were adjusted at different pH values (2, 4, 6, 8, 10, and 12), using 0.1 M HCl or 0.1 M NaOH. Then, 0.05 g Mn_3O_4 nanoparticles was added to each bottle and shacked for 2 days. As illustrated in Fig. 5, the intersection point of the initial pH and final pH is called the pHpzc. The pHpzc for Mn_3O_4 NPs is 4.6, which confirmed the results reported by Durmus et al. (2010). At a pH higher than 4.6, the surface of Mn_3O_4 NPs becomes negatively charged which gives high preference for the binding between Mn_3O_4 NPs and the elements under study [Eu(III) and Gd(III)].

Batch sorption investigations

The sorption of gadolinium and europium ions from aqueous solution with Mn_3O_4 nanoparticles was affected by different factors such as pH, shaking time, initial metal concentration, and temperature. These factors were studied in a batch adsorption technique.

Effect of hydrogen ion concentration (pH)

The uptake of Gd(III) and Eu(III) ions from aqueous solutions using Mn_3O_4 NPs was assessed in the ranges of pH from 2.0 to 10.0, which is shown in Fig. 6. It was indicated that the adsorption of Gd(III) and Eu(III) ions on Mn_3O_4 NPs is increasing by increasing the pH. The maximum removal percentages were achieved at pH 5.0 for Gd(III) and Eu(III). The adsorption of Gd(III) and Eu(III) above pH 5.0 decreased due to precipitation of both elements.

Metal ion concentration effect

The sorption capacity of Mn_3O_4 NPs for the uptake of Gd(III) and Eu(III) from aqueous solution with initial concentration from 20 to 800 mg/L at pH value 5.0 for Gd(III) and Eu(III) is shown in Fig. 7. The sorption capacity Mn_3O_4 NPs was noticed to increase to a definite value as a result of the increase in the metal concentration from 20 to 800 mg/L,

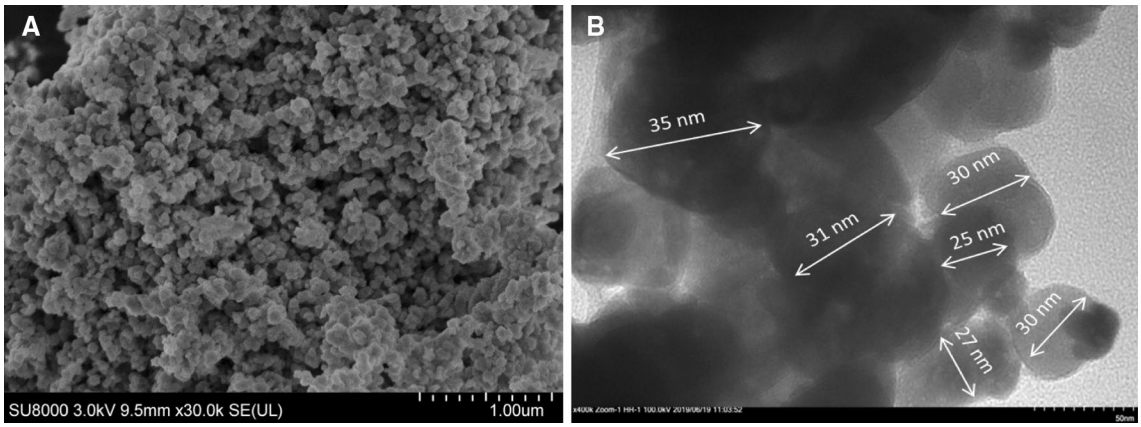

Fig. 4 **a** FE-SEM image and **b** HR-TEM image of the as-prepared Mn_3O_4 NPs

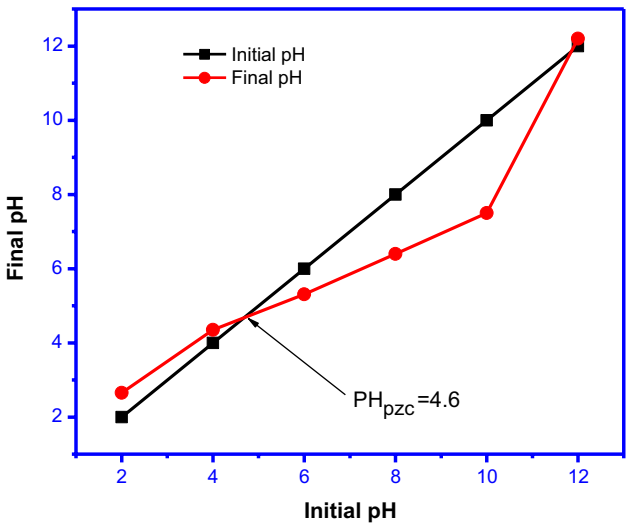

Fig. 5 pHpzc of Mn_3O_4 nanoparticles

and this behavior can be explained by the progressive increase in the electrostatic interaction between Gd(III) and Eu(III) ions and Mn_3O_4 NPs active sites (Laraous et al. 2005). It is obvious that the maximum adsorption capacity of Mn_3O_4 NPs is acquired at concentration of 300 mg/L for both Gd(III) and Eu(III). Slow stability in the capacity was observed with the increase in Gd(III) and Eu(III) concentration, because all the active sites on the surface of Mn_3O_4 NPs were saturated, and thus, no Gd(III) and Eu(III) could be adsorbed (Sayed et al. 2017). The sorption capacity of Mn_3O_4 NPs for Gd(III) and Eu(III) was 11.7 and 25.3 mg/g, respectively.

Shaking time effect

The sorption of Gd(III) and Eu(III) by Mn_3O_4 NPs was investigated within shaking time from 30 to 600 min as it is indicated in Fig. 8. The results showed that the uptake of the Gd(III) and Eu(III) includes two successive stages; the

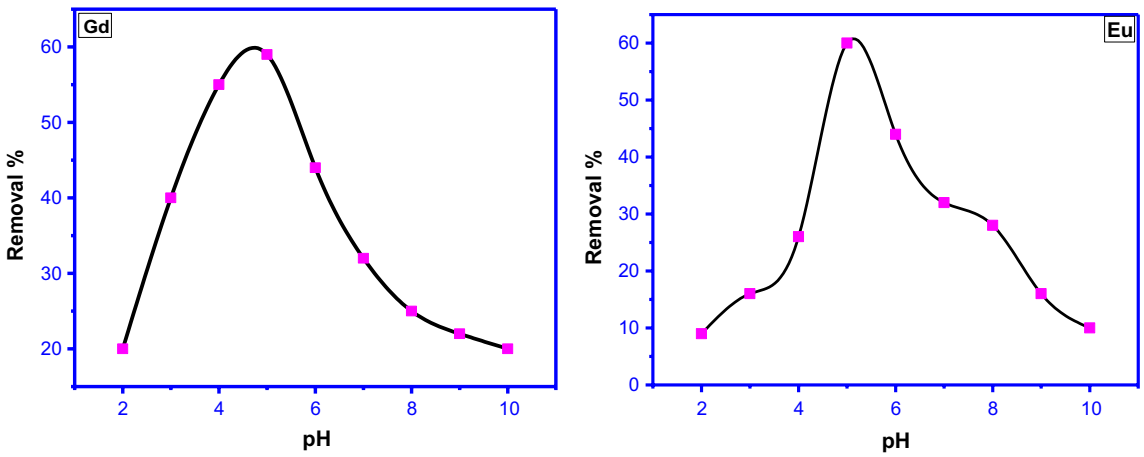

Fig. 6 Effect of pH on the sorption of Gd(III) and Eu(III) ions by Mn_3O_4 NPs (C_o = 100 mg/l, V = 20 ml, W = 0.1 g, time = 24 h, T = 25 °C, and shaking speed = 300 rpm)

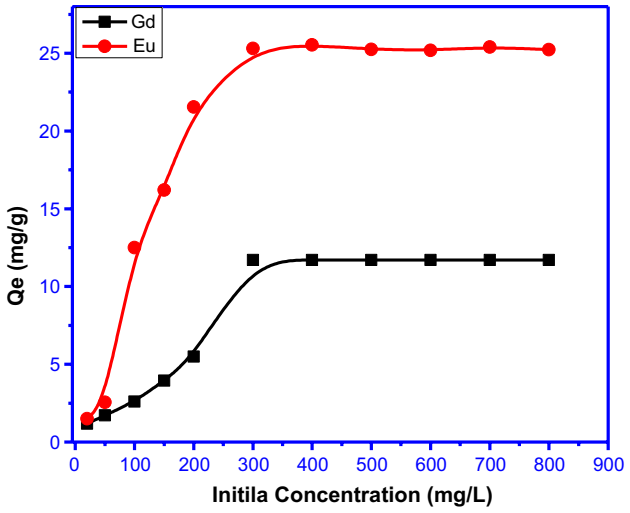

Fig. 7 Effect of initial Gd(III) and Eu(III) concentration on the sorption capacity of Mn_3O_4 NPs [W = 0.1 g, time = 24 h, V = 20 ml, T = 25 °C, pH = 5.0 (Gd) and pH = 5.0 (Eu), and shaking speed = 300 rpm]

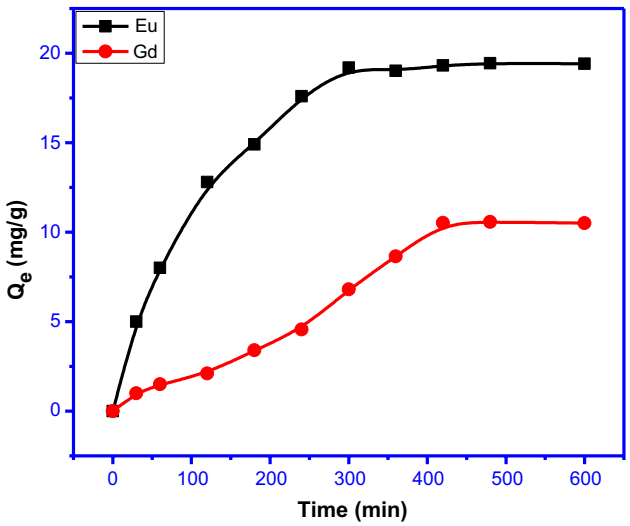

Fig. 8 Shaking time effect on the sorption of Gd(III) and Eu(III) ions by Mn_3O_4 NPs [W = 0. 1 g, C_o = 300 ppm, V = 20 ml, T = 25 °C, pH = 5.0 (Eu) and pH = 5.0 (Gd), and shaking speed = 300 rpm]

first stage includes fast uptake throughout the first 300 min because of the presence of many active sites on Mn_3O_4 NPs surface. The second stage indicates the equilibrium of sorption process at about 300 min. These two discrete steps were also identified by Burke et al. (2013). The equilibrium time for sorption of Gd(III) and Eu(III) was optimized at 300 and 420 min, respectively.

Kinetic modeling The mechanism of adsorption with time was discussed through pseudo-first-order model, pseudo-second-order model, and intraparticle diffusion model.

Pseudo-first-order model The Legergren pseudo-first-order kinetic model can be expressed by the following equation (Kowanga et al. 2016):

$$\mathrm{Log}(q_e - q_t) = \log q_e - k_1 t\,/2.303, \tag{7}$$

where q_e is the amount of Gd(III) or Eu(III) adsorbed at equilibrium per unit mass of Mn_3O_4 NPs (mg/g), k_1 is the rate constant of pseudo-first-order equation (min^{-1}), and q_t is the amount adsorbed of Gd(III) or Eu(III) per unit mass of Mn_3O_4 NPs (mg/g) at any time t. We can plot log ($q_e - q_t$) versus t, as shown in Fig. S1, from the slope and intercept; q_e and $\boldsymbol{t}$ can be calculated.

Pseudo-second-order model The linear form of pseudo-second-order equation can be expressed by the following equation (Plazinski et al. 2013):

$$t/q_t = 1/k_2 q_e^2 + t/q_e, \tag{8}$$

where k_2 is rate constant of the pseudo-second-order equation (g/mg/min); similarly, q_e and q_t as defined in case of pseudo-first-order. Plotting of t/q_t against t gives the parameters of q_e and k_2, as illustrated in Fig. S2. Referring to Table S2, it is observed that the correlation coefficients (R^2) of Gd(III) and Eu(III) were in most cases greater than that for the pseudo-first-order model. Accordingly, the experimental data of the adsorption kinetics were matched well with the pseudo-second-order kinetic model. Besides, the theoretical sorption capacity (q_e, calculated) and the experimental sorption capacity (q_e, experimental) values were in good match for second-order model, while for first order, they are different. These results recommended that the adsorption of Gd^{3+} and Eu^{3+} ions on Mn_3O_4 NPs follows the kinetic model of the second-order type.

Intraparticle diffusion model The metal ion transfers from the liquid phase to the solid phase within the sorption process in many steps; film diffusion, pore diffusion, and particle diffusion (Srivastava et al. 2006).

The intraparticle diffusion model (IPD) is expressed by the following equation:

$$q_t = k_{id} t^{0.5} + C, \tag{9}$$

where C = thickness of the boundary layer, k_{id} = the constant of intraparticle diffusion [mg/(g $min^{1/2}$)], and q_t = the amount of Gd(III) or Eu(III) adsorbed on mass unit of Mn_3O_4 NPs (mg/g) at time t. From the plot of q_t against $t^{0.5}$ as illustrated in Fig. S3, k_{id} was calculated from the slope (Shrihari et al. 2005).

The IPD kinetics model was applied in predicting the rate-limiting step which is film diffusion or intraparticle diffusion. The rate-controlling step will be intraparticle diffusion, if the plot of q_t as opposed to $t^{0.5}$ passes through

the point of origin (Özcan and Özcan 2005). From the data revealed in Table S2, it is observed that the plots in this study show a multi-linearity; first, the plots show an initial rapid portion and then horizontal linear portion. The first sharp step of the plots is as a result of the external surface sorption of Gd(III) or Eu(III) on Mn_3O_4 NPs. The second part of the plot recommends the gradual adsorption step with controlled intraparticle diffusion. As the lines do not pass through the point of origin, we can conclude that the intraparticle diffusion is not the only rate-regulating step (Mall et al. 2005). This trend of IDP model was also similarly reported by Liu et al. (2013) and Fierro et al. (2008).

Adsorption isotherms The adsorption isotherm models illustrate the relation between the amount adsorbed by a unit mass of sorbent and the amount of metal ion remaining in the solution at equilibrium. The sorption isotherm of Mn_3O_4 NPs was studied in terms of the two sorption isotherms: Freundlich and Langmuir models. These models are applied to determine the maximum capacity of Gd(III) and Eu(III) sorption by Mn_3O_4 NPs. Fitting of the isotherm to the experimental data was evaluated related to the correlation coefficient R^2, i.e., the isotherm which gives R^2 value close to one is considered to give the best fit. The adsorption isotherm studies were investigated at adsorbent weight (0.1 g of Mn_3O_4 NPs), temperature (25 °C), varying Gd(III) and Eu(III) concentrations (20–400 mg/l) and pH = 5.0 (Eu) and pH = 4.0 (Gd) (Fierro et al. 2008; Galhoum et al. 2017).

Freundlich isotherm The Freundlich isotherm model is widely applied to illustrate the multilayer sorption on heterogeneous surfaces (Gad et al. 2014).

The Freundlich isotherm is expressed using the following equation:

$$\log q_e = \log K_F + \frac{1}{n} \log C_e, \tag{10}$$

where C_e is the concentration of Gd(III) or Eu(III) at equilibrium (mg/l), q_e is the amount of Gd(III) or Eu(III) adsorbed using 1 g of Mn_3O_4 NPs (mg/g), K_F is the Freundlich constant (mg/g), and $1/n$ is the adsorption intensity (g/l).

Langmuir isotherm The model of Langmuir isotherm is applicable in case of sorption on homogenous surfaces. This isotherm assumes that there are a certain number of active sites on the surface of the adsorbent, and thus, it includes formation of monolayer adsorption (Gad et al. 2014). The linear equation of this model is shown in Eq. (11):

$$\frac{C_e}{q_e} = \frac{1}{Q_o b} + \frac{C_e}{Q_o}, \tag{11}$$

where q_e is the amount of Gd(III) or Eu(III) adsorbed per mass unit of Mn_3O_4 NPs (mg/g), C_e is the Gd(III) or Eu(III) concentration at equilibrium (mg/L), b is the constant of Langmuir isotherm (L/mg), and Q_o is the theoretical adsorption capacity (mg/g) (Sadia et al. 2013). Plotting of C_e/q_e against C_e provides linear relation as indicated in Fig. S4; from the slope Q_o, is obtained and b is obtained from intercept.

As shown in Table 1, Figs. S4 and S5, it is concluded that the adsorption pattern of Gd^{3+} and Eu^{3+} on Mn_3O_4 NPs was fitted well with the Langmuir model with R^2 values of 0.996 and 0.997, which is higher than the case of Freundlich model, and it is seen that the adsorption of Gd(III) and Eu(III) is favorable. The high R^2 values obtained from the Langmuir model revealed fitness of this model in expressing equilibrium sorption data, in addition to the adsorption capacity obtained from the Langmuir isotherm for Gd(III) is 12.6 mg/g which matched well with the experimental data (11.7 mg/g). Furthermore, the calculated sorption capacity from Langmuir model for Eu(III) is 26.8 mg/g, and this value is matched well with the experimental capacity (25.3 mg/g). In addition, the fitness of the model shows that Eu(III) and Gd(III) are adsorbed as monolayer onto Mn_3O_4 NPs surface with a distinct number of active sites, which are homogeneously distributed on the surface of Mn_3O_4 NPs (Mahmoud 2015). The values of K_F and n show the increase of negative charge on the surface which enhances the electrostatic forces between Mn_3O_4 NPs and Gd ions and Eu ions leading to increasing in the adsorption of Gd^{3+} and Eu^{3+} (Chen 2015).

Effect of temperature

The effect of temperature on the sorption of Eu^{3+} and Gd^{3+} from aqueous solutions was studied by varying the temperature between 25 and 65 °C. The data given in Fig. 9 showed that adsorption of these metal ions by Mn_3O_4 NPs increased with increase in temperature. The increase in adsorption with increasing temperature up to 65 °C is due to increased penetration of Eu^{3+} and Gd^{+} ions inside micropores at

Table 1 Langmuir and Freundlich parameters for sorption of Eu(III) and Gd(III) ions onto Mn_3O_4 NPs

Sample	Element	Langmuir model			Freundlich model		
		Q_o (mg/g)	B (L/mg)	R^2	K_F (mg/g)	N	R^2
Mn_3O_4	Eu(III)	26.8	0.03	0.997	1.19	1.63	0.949
Nanoparticles	Gd(III)	12.6	0.0195	0.996	0.26	1.44	0.972

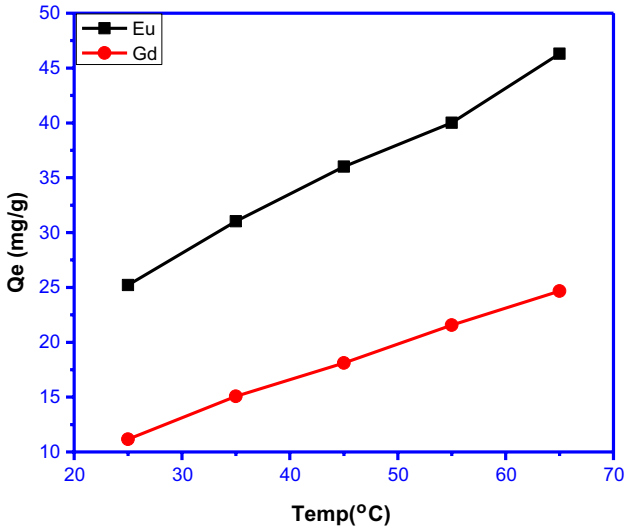

Fig. 9 Effect temperature on the sorption of Gd(III) and Eu(III) ions by Mn_3O_4 NPs [W = 0. 1 g, C_o = 300 ppm, V = 20 ml, pH = 5.0 (Eu) and (Gd), shaking time = 300 min for Eu(III) and 420 min for Gd(III), and shaking speed = 300 rpm]

higher temperatures or the creation of new active sites (Al-Degs et al. 2008).

Thermodynamic studies The sorption of Eu(III) and Gd(III) by Mn_3O_4 NPs increases by raising the temperature from 25 to 65 °C and this behavior approved the endothermic nature of the adsorption process. The changes in standard free energy (ΔG), enthalpy (ΔH), and entropy (ΔS) of adsorption were calculated from the following equations:

$$\Delta G = -RT \ln K_C, \tag{12}$$

where R is the gas constant, K_C the equilibrium constant, and T the temperature in K. The K_C value is calculated by the following equation:

$$K_c = \frac{C_A}{C_E}, \tag{13}$$

where C_A is the equilibrium concentration of Eu(III) and Gd(III) on Mn_3O_4 NPs (mg/L) and C_E is the equilibrium concentration of Eu(III) and Gd(III) in solution. The enthalpy changes (ΔH) for the process equilibrium and entropy (ΔS) can be calculated from van't Hoff equation given by the following equation (Gad and El-Sayed 2009):

$$\ln K_C = \frac{-\Delta H}{RT} + \frac{\Delta S}{R}. \tag{14}$$

By plotting $\ln K_c$ against $1/T$, straight line is obtained as indicated in Fig. S6. The values of ΔS and ΔH can be obtained from the slope and intercept, respectively. As indicated in Table 2, the values of ΔH and ΔS for the sorption of Eu(III) and Gd(III) onto Mn_3O_4 NPs were found to be 23.1 kJ/mol and 65.1 J/mol k for Gd(III) and 30.9 kJ/mol and 100.9 J/mol K for Eu(III), respectively. The positive value of ΔH value shows the endothermic nature of the sorption process, while the positive value of ΔS illustrates the increase in the randomness of the system. The negative values of ΔG show the spontaneous nature of the sorption of Gd(III) and Eu(III) by Mn_3O_4 NPs.

Table 2 Thermodynamic parameters for sorption of Eu(III) and Gd(III) ions onto Mn_3O_4 NPs

Element	Temp. (K)	ΔG (kJ/mol)	ΔH (kJ/mol)	ΔS (J/mol K)	R^2
Gd(III)	298	− 19.5	23.1	65.5	0.992
	308	− 20.1			
	318	− 20.8			
	328	− 21.5			
	338	− 22.1			
Eu(III)	298	− 30.0	30.9	100.9	0.981
	308	− 31.0			
	318	− 32.0			
	328	− 33.1			
	338	− 34.1			

Possible preconcentration of Eu(III) and Gd(III)

Preconcentration of metal ion is frequently applied to any metal ion of low concentration before its measurement by any analytical technique. The preconcentration process means that increasing the concentration of analyte by transferring this analyte from large volume solution to small volume solution. The aim of this preconcentration process is increasing sensitivity, lowering detection limit of determination techniques, and removal of the interfering ions from matrix. There are many techniques used for preconcentration of analytes from aqueous solutions such as evaporation, solid-phase extraction, ion exchange, solvent extraction, and co-precipitation. SPE can be applied in different ways, one of these is applied here where the sorbent is added into the sample matrix and shaken for certain time, and then, it is separated from the solution by filtration or centrifugation. To determine the preconcentration factor of Mn_3O_4 NPs, the effect of eluent type and sample volume should be carried out. Preconcentration factor can be defined from the relation given in Eq. (15):

$$\text{Preconcentration factor} = \frac{\text{highest sample volume}}{\text{lowest eluion volume}}. \tag{15}$$

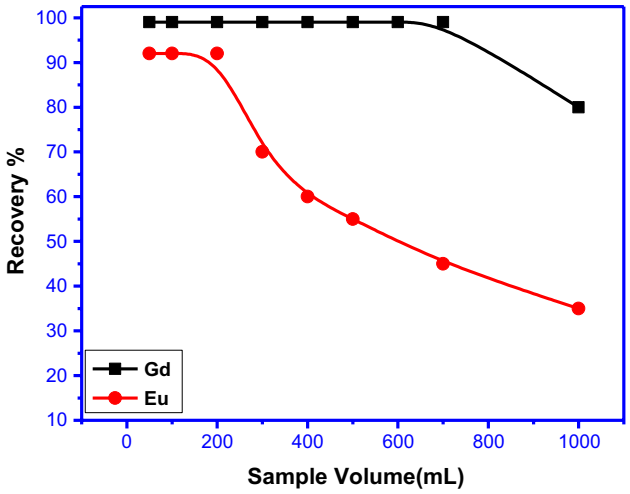

Fig. 10 Sample volume effect on the uptake of Eu(III) and Gd(III) from aqueous solutions [W = 0. 1 g, Gd(III) concentration = 20 ppm and Eu(III) concentration = 5 ppm, pH = 5.0 (Eu) and pH = 5.0 (Gd), shaking speed = 300 rpm, and shaking time = 300 min for Eu(III) and 420 min for Gd(III)]

Effect of eluent type

Desorption of the retained Eu(III) and Gd(III) from Mn_3O_4 NPs was experimented using different eluents like hydrochloric acid, nitric acid, and EDTA with different concentrations.

From the results given in Fig. S7, it can be concluded that 2.0 M HNO_3 was found to be the best eluent compared to other solvents for desorption of Eu(III) and Gd(III) from the surface of Mn_3O_4 NPs.

Effect of the sample volume

It is important to optimize sample volume to acquire a high preconcentration factor to analyze real samples. The effect of solution volume was assessed by preconcentrating different volumes (50–1000 mL) of Gd(III) (20.0 ppm) and Eu(III) (5.0 ppm). Regarding to the results specified in Fig. 10, it can be concluded that when the aqueous solution volume of Gd(III) was up to 700 mL, the recovery percentage was above 95%. Thus, 700 mL was believed to be the highest enrichment sample volume. For Eu(III), at higher sample volumes more than 200 ml, the recovery % decreased gradually. Hence, the best sample volume for Eu(III) was found to be 200 mL. The preconcentration factor is determined as the ratio of the highest sample volume and the lowest final volume (Elvan et al. 2013). As the final volume of eluent for Gd(III) and Eu(III) was 10.0 mL, preconcentration factor of 70 was gained for Gd(III) and of 20 for Eu(III).

Conclusion

In the present study, Mn_3O_4 NPs were successfully synthesized by simple co-precipitation method. The synthesized Mn_3O_4 NPs were used for the first time as a new sorbent for the sorption and preconcentration of Gd(III) and Eu(III) from aqueous solutions. The experimental data for the sorption of Gd(III) and Eu(III) using Mn_3O_4 NPs are more fitted to Langmuir isotherm model with maximum sorption capacity reached 26.8 and 12.6 mg/g for Eu(III) and Gd(III), respectively. The adsorption kinetics data were found to follow the pseudo-second-order model and the results obtained from intraparticle diffusion model exposed that the overall process was jointly controlled by external mass transfer and intraparticle diffusion. All the obtained results in this study suggest that nanosized Mn_3O_4 is a favorable sorbent for uptake of Gd(III) and Eu(III) from aqueous solutions. Thus, this paper shows that Mn_3O_4 NPs is a promising sorbent for a selective separation of Gd^{3+} and Eu^{3+} from aqueous solutions with preconcentration factor up to 70 for Gd(III) and up to 20 for Eu(III).

References

Aghamohammadhasan M, Ghashamsham V, Ghorbani M, Chamsaz M, Masrournia M, Pedramrad T, Akhlaghi H (2017) Preconcentration of gadolinium ion by solidification of floating organic drop microextraction and its determination by UV–Vis Spectrophotometry. Euras J Anal Chem 12(8):1621–1629

Al-Degs YS, El-Barghouthi MI, El-Sheikh AH, Walker GM (2008) Effect of solution pH, ionic strength, and temperature on adsorption behavior of reactive dyes on activated carbon. Dyes Pigm 77(1):16–23

Al Lafi AG, Al Abdullah J (2015) Cesium and cobalt adsorption on synthetic nano manganese oxide: a two dimensional infra-red correlation spectroscopic investigation. J Mol Struct 1093:13–23

Alizadeh T, Amjadi S (2013) Synthesis of nano-sized Eu^{3+}-imprinted polymer and its application for indirect voltammetric determination of europium. Talanta 106:431–439

Bartolini ME, Pekar J, Chettle DR, McNeill F, Scott A, Sykes J, Moran GR (2003) An investigation of the toxicity of gadolinium based MRI contrast agents using neutron activation analysis. Magn Reson Imaging 21(5):541–544

Bastami TR, Entezari MH (2010) Sono-synthesis of Mn_3O_4 nanoparticles in different media without additives. Chem Eng J 164(1):261–266

Belkhedkar MR, Ubale AU (2014) Physical properties of nanostructured Mn_3O_4 thin films synthesized by SILAR method at room temperature for antibacterial application. J Mol Struct 1068:94–100

Burke DM, Morris MA, Holmes JD (2013) Chemical oxidation of mesoporous carbon foams for lead ion adsorption. Sep Purif Technol 104:150–159

Chen X (2015) Modeling of experimental adsorption isotherm data. Information 6(1):14–22

Chen Z, Pan D, Li Z, Jiao Z, Wu M, Shek CH, Lai JK (2014) Recent advances in tin dioxide materials: some developments in thin films, nanowires, and nanorods. Chem Rev 114(15):7442–7486

Dalvand A, Nabizadeh R, Ganjali MR, Khoobi M, Nazmara S, Mahvi AH (2016) Modeling of Reactive Blue 19 azo dye removal from colored textile wastewater using L-arginine-functionalized Fe_3O_4 nanoparticles: optimization, reusability, kinetic and equilibrium studies. J Magn Magn Mater 404:179–189

Dhaouadi H, Ghodbane O, Hosni F, Touati F (2012) Mn_3O_4 nanoparticles: synthesis, characterization and dielectric properties. ISRN Spectrosc 1:1–8

Dubal DP, Dhawale DS, Gujar TP, Lokhande CD (2011) Effect of different modes of electrodeposition on supercapacitive properties of MnO_2 thin films. Appl Surf Sci 257(8):3378–3382

Durmus Z, Tomas M, Baykal A, Kavas H, Altincekic TG, Toprak MS (2010) The effect of neutralizing agent on the synthesis and characterization of Mn_3O_4 nanoparticles. Russ J Inorg Chem 55:1947–1952

El-Sofany E (2008) Removal of lanthanum and gadolinium from nitrate medium using Aliquat-336 impregnated onto Amberlite XAD-4. J Hazard Mater 153(3):948–954

Elvan H, Ozdes D, Duran C, Sahin D, Tufekci M, Bahadir Z (2013) Separation and preconcentration of copper in environmental samples on Amberlite XAD-8 resin after complexation with a carbothioamide derivative. Quími Nova 36(6):831–835

Fedyunina N, Ossipov I, Seregina M, Bolshov M, Statkus M, Tsysin G (2012) Determination of rare earth elements in rock samples by inductively coupled plasma mass-spectrometry after sorption preconcentration using Pol-DETATA sorbent. Talanta 102:128–131

Fierro V, Torné-Fernández V, Montané D, Celzard A (2008) Adsorption of phenol onto activated carbons having different textural and surface properties. Microporous Mesoporous Mater 111(1–3):276–284

Gad HM, El-Sayed AA (2009) Activated carbon from agricultural by-products for the removal of Rhodamine-B from aqueous solution. J Hazard Mater 168(2–3):1070–1081

Gad HMH, Ali MMS, Zaher WF, El-Sofany EA, Abo-El-Enein SA (2014) Application of Olive Stone based activated carbon in the sorption of lanthanum (III) ions from aqueous solution. Arab J Nucl Sci Appl 47(3):67–79

Gad HM, Hamed MM, Eldahab HA, Moustafa ME, El-Reefy SA (2017) Radiation-induced grafting copolymerization of resin onto the surface of silica extracted from rice husk ash for adsorption of gadolinium. J Mol Liq 231:45–55

Galhoum AA, Hassan KM, Desouky OA, Masoud AM, Akashi T, Sakai Y, Guibal E (2017) Aspartic acid grafting on cellulose and chitosan for enhanced Nd(III) sorption. React Funct Polym 113:13–22

Huittinen N, Rabung T, Lützenkirchen J, Mitchell SC, Bickmore BR, Lehto J, Geckeis H (2009) Sorption of Cm(III) and Gd(III) onto gibbsite, α-Al $(OH)_3$: a batch and TRLFS study. J Colloid Interface Sci 332(1):158–164

Kanna M, Wongnawa S, Sherdshoopongse P, Boonsin P (2005) Adsorption behavior of some metal ions on hydrated amorphous titanium dioxide surface. Adsorption 27(5):1018–1026

Karadas C, Kara D, Fisher A (2011) Determination of rare earth elements in seawater by inductively coupled plasma mass spectrometry with off-line column preconcentration using 2,6-diacetylpyridine functionalized Amberlite XAD-4. Anal Chim Acta 689:184–189

Kazakov AG, Aliev RA, Bodrov AY, Priselkova AB, Kalmykov SN (2018) Separation of radioisotopes of terbium from a europium target irradiated by 27 MeV α-particles. Radiochim Acta 106(2):135–140

Kowanga KD, Gatebe E, Mauti GO, Mauti EM (2016) Kinetic, sorption isotherms, pseudo-first-order model and pseudo-second-order model studies of Cu (II) and Pb(II) using defatted *Moringa oleifera* seed powder. J Phytopharmacol 5(2):71–78

Laraous S, Meniai AH, Bencheikh LM (2005) Experimental study of the removal of copper from aqueous solutions by adsorption using sawdust. Desalination 185:483–490

Lei S, Tang K, Fang Z, Sheng J (2007) One-step synthesis of colloidal Mn_3O_4 and γ-Fe_2O_3 nanoparticles at room temperature. J Nanopart Res 9(5):833–840

Li Y, Hu B (2010) Cloud point extraction with/without chelating agent on-line coupled with inductively coupled plasma optical emission spectrometry for the determination of trace rare earth elements in biological samples. J Hazard Mater 174(1–3):534–540

Liang P, Chen X (2005) Preconcentration of rare earth elements on silica gel loaded with 1-phenyl-3-methyl-4-benzoylpyrazol-5-one prior to their determination by ICP-AES. Anal Sci 21(10):1185–1188

Liang P, Liu Y, Guo L (2005) Determination of trace rare earth elements by inductively coupled plasma atomic emission spectrometry after preconcentration with multiwalled carbon nanotubes. Spectrochim Acta Part B 60:125–129

Liu YG, Ting L, He ZB, Li TT, Hui W, Hu XJ, Yuan HE (2013) Biosorption of copper (II) from aqueous solution by Bacillus subtilis cells immobilized into chitosan beads. T Nonferr Metal Soc 23(6):1804–1814

Liu Y, Wei J, Tian Y, Yan S (2015) The structure–property relationship of manganese oxides: highly efficient removal of methyl orange from aqueous solution. J Mater Chem A 3(37):19000–19010

Mahmoud MA (2015) Kinetics and thermodynamics of aluminum oxide nanopowder as adsorbent for Fe(III) from aqueous solution. J Basic Appl Sci 4(2):142–149

Mall ID, Srivastava VC, Agarwal NK, Mishra IM (2005) Removal of congo red from aqueous solution by bagasse fly ash and activated carbon: kinetic study and equilibrium isotherm analyses. Chemosphere 61(4):492–501

Mallah MH, Shemirani F, Maragheh MG (2008) Use of dispersive liquid-liquid microextraction for simultaneous preconcentration of samarium, europium, gadolinium and dysprosium. J Radioanal Nucl Chem 278:97–102

Mansournia M, Azizi F, Rakhshan N (2015) A novel ammonia-assisted method for the direct synthesis of Mn_3O_4 nanoparticles at room temperature and their catalytic activity during the rapid degradation of azo dyes. J Phys Chem Solids 80:91–97

Moyer E, McCarthy W (1969) Evaluation of electron spin resonance for quantitative determinations of gadolinium, chromium, iron, copper and manganese. Anal Chim Acta 48:79

Ohashi A, Hashimoto T, Imura H, Ohashi K (2007) Cloud point extraction equilibrium of lanthanum(III), europium(III) and lutetium(III) using di(2-ethylhexyl)phosphoric acid and Triton X-100. Talanta 73:893–898

Othersen J, Maize J, Woolson R, Budisavljevic M (2007) Nephrogenic systemic fibrosis after exposure to gadolinium in patients with renal failure. Nephrol Dial Transpl 22(11):3179–3185

Özcan A, Özcan AS (2005) Adsorption of Acid Red 57 from aqueous solutions onto surfactant-modified sepiolite. J Hazard Mater 125(1–3):252–259

Person P, Andersson P, Zhang J, Porcelli D (2011) Determination of Nd isotopes in water: a chemical separation technique for extracting Nd from seawater using a chelating resin. Anal Chem 83:1336–1341

Plazinski W, Dziuba J, Rudzinski W (2013) Modeling of sorption kinetics: the pseudo-second order equation and the sorbate intraparticle diffusivity. Adsorption 19(5):1055–1064

Pyrzynska K (2013) Use of nanomaterials in sample preparation. TrAC, Trends Anal Chem 43:100–108

Rufus AL, Kumar PS, Jeena K, Velmurugan S (2018) Removal of gadolinium, a neutron poison from the moderator system of nuclear reactors. J Hazard Mater 342:77–84

Sadia M, Jan MR, Shah J, Greenway GM (2013) Simultaneous preconcentration and determination of nickel and cobalt using functionalised mesoporous silica spheres by ICP-OES. Int J Environ Anal Chem 93(14):1537–1556

Sartape AS, Mandhare AM, Jadhav VV, Raut PD, Anuse MA, Kolekar SS (2017) Removal of malachite green dye from aqueous solution with adsorption technique using *Limonia acidissima* (wood apple) shell as low cost adsorbent. Arab J Chem 10:S3229–S3238

Sayed MA, Helal AI, Abdelwahab SM, Aly HF (2017) Sorption of cesium from aqueous solutions by some Egyptian pottery materials. Appl Clay Sci 139:1–8

Sherin JS, Thomas JK, Suthagar J (2014) Combustion Synthesis and magnetic studies of hausmannite, Mn_3O_4, nanoparticles. Int J Eng Res Develop 10:34–41

Shizhong C, Mingfa X, Dengbo L, Xilin Z (2007) Carbon nanofibers as solid-phase extraction adsorbent for the preconcentration of trace rare earth elements and their determination by inductively coupled plasma mass spectrometry. Anal Lett 40:2105–2115

Shrihari V, Madhan S, Das A (2005) kinetics of phenol sorption by Raw Agrowastes. Appl Sci 6(1):47–50

Shrividhya T, Ravi G, Mahalingam T, Hayakawa Y (2014) Synthesis and study on structural, morphological and magnetic properties of nanocrystalline manganese oxide. Int J Sci Eng Appl 5:13–16

Singha M, Pal S, Hareendran KN, Roy SB (2014) Poly-hydroxamic acid (PHA) matrix for gadolinium pre-concentration and removal. J Radioanal Nucl Chem 302:961–966

Srivastava VC, Swamy MM, Mall ID, Prasad B, Mishra IM (2006) Adsorptive removal of phenol by bagasse fly ash and activated carbon: equilibrium, kinetics and thermodynamics. Colloids Surf A 272(1–2):89–104

Sun Y, Wang Q, Chen C, Tan X, Wang X (2012) Interaction between Eu(III) and graphene oxide nanosheets investigated by batch and extended X-ray absorption fine structure spectroscopy and by modeling techniques. Environ Sci Technol 46:6020–6027

Vázquez-Olmos A, Redón R, Rodríguez-Gattorno G, Mata-Zamora ME, Morales-Leal F, Fernández-Osorio AL, Saniger JM (2005) One-step synthesis of Mn_3O_4 nanoparticles: structural and magnetic study. J Colloid Interface Sci 291(1):175–180

Zamani HA, Mohammadhosseini M, Haji-Mohammadrezazadeh S, Faridbod F, Ganjali MR, Meghdadi S, Davoodnia A (2012) Gadolinium (III) ion selective sensor using a new synthesized Schiff's base as a sensing material. Mater Sci Eng, C 32(4):712–717

Zhang P, Zhan Y, Cai B, Hao C, Wang J, Liu C, Chen Q (2010) Shape-controlled synthesis of Mn3O 4 nanocrystals and their catalysis of the degradation of methylene blue. Nano Res 3(4):235–243

Zhang Y, Zhong C, Zhang Q, Chen B, He M, Hu B (2015) Graphene oxide-TiO_2 composite as a novel adsorbent for the preconcentration of heavy metals and rare earth elements in environmental samples followed by on-line inductively coupled plasma optical emission spectrometry detection. RSC Adv 5:5996–6005